Climate Dynamics (1997) 13: 521–532

Climate Dynamics

Comparative energetics analysis of CCM2 with different horizontal resolutions

A. Hasegawa,[1] H. L. Tanaka,[1] H. Hirakuchi,[2] S. Taguchi[3]

[1] Institute of Geoscience, University of Tsukuba, Japan
[2] Central Research Institute of Electric Power Industry, Japan
[3] National Institute for Resources and Environment, Japan

Received: 15 July 1996/Accepted: 3 January 1997

Abstract. Comprehensive global energetics analysis is carried out for the NCAR CCM2 with different horizontal resolutions of R15, T42, T63, and T106 to assess the effect of various model truncations on the global energetics characteristics in climate models. Both the energy levels and energy transformations are examined over the zonal wave number domain during a northern winter and summer. In addition to the simulated atmosphere, the ECMWF global analysis during 1986 to 1990 is analyzed for comparison using the same diagnostic scheme. Previous studies have revealed that zonal kinetic energy is supplied by synoptic disturbances in terms of the zonal-wave interactions of kinetic energy. According to our result, however, such an energy flow from eddies to zonal motions is valid only for zonal wave numbers up to about 30. We find that the zonal-wave interactions of kinetic energy change sign beyond wave number 30 where the energy is transformed from zonal to eddies for both the ECMWF and CCM2-T106. The large-scale zonal motions are diffusive against the short waves beyond wave number 30, which may well be parameterized by various forms of the diffusion schemes. We suggest from this result that the atmospheric disturbances with wave numbers lower than 30 are necessary to represent accurately the two-way interactions between zonal and eddy motions, because these waves can actively influence the behavior of the zonal motions. Based on this finding, we suggest that the model resolution of R15 is inadequate for climate studies from the energetics point of view, and that resolution of T42 is the minimum requirement to represent the general circulation adequately. Some other discrepancies are discussed in detail for the coarse resolution climate models.

Correspondence to: H. L. Tanaka
E-mail: tanaka@atm.geo.tsukuba.ac.jp

1 Introduction

The central activity in modern climate research is the conduct of climate model simulations with various model resolutions. Present climate models, however, have relatively coarse horizontal and vertical resolutions compared with the operational numerical weather prediction models due to the inevitable restrictions in computing capability. In coarse general circulation models, for example R15, the spectral truncation at the medium wave number imposes unrealistic and undesirable restrictions in the spectral energy transfer. For instance, the nonlinear energy cascade within the model atmosphere must terminate at the imposed truncation wave number. In reality, of course, there is no artificial spectral boundary, so the energy input at the global scale is transferred to the dissipation range without interruption. In spite of many uncertainties associated with such coarse resolution models, they alone afford a scientific means for quantitatively examining the range of future climate changes that may result from anthropogenic activities (e.g., Giorgi and Mearns 1991; Manabe and Stouffer 1996). Hence, the examination of the uncertainty associated with the artificial spectral boundary at the truncation wave number is an important research subject in predicting the climate equilibrium state. Williamson et al. (1995) compare the basic variables for the National Center for Atmospheric Research (NCAR) Community Climate Model version 2 (hereafter, CCM2) with different horizontal resolutions. However, Williamson et al. (1995) are still unable to clarify an appropriate resolution for climate studies. Thus, the evaluation of the energy transfer between global- and small-scale motions is an important subject to assess the basic performance of existing climate models with different model resolutions.

A standard approach for the traditional global energetics analysis may be the spectral energetics in terms of a one-dimensional wave number decomposition introduced by Saltzman (1957, 1970). Many diagnostic results have been reported after Saltzman (e.g., by Oort, 1964; Tenenbaum 1976; Tsay and Kao 1978; Kao and Chi 1978; Kung and Tanaka, 1983, 1984; Kung and Baker 1986; Arpe et al. 1986; Kung 1988). Kung and Tanaka (1983, 1984) reported the first comprehensive analysis of global

energy levels and energy transformations in the zonal wave number domain, using the extensive world-wide observation of the First GARP (Global Atmospheric Research Programme) Global Experiment (FGGE). According to their observational analysis, the zonal jet stream in mid-latitudes is maintained by the barotropic conversion represented by zonal-wave interactions of kinetic energy from synoptic disturbances to the zonal mean flow. The nonlinear wave-wave interactions of kinetic energy indicate energy flows from synoptic waves to both planetary waves and short waves. The kinetic energy of the synoptic disturbances is maintained by the baroclinic conversion from $P(n)$ to $K(n)$, induced by the baroclinic instability. Evaluating those energetics terms for climate models with various model resolutions is meaningful to assess the effect of the artificial model truncations.

Another motivation for the spectral energetics analysis for various model resolutions comes from the validation of developing a limited area model (LAM) nested in a general circulation model (GCM) for climate prediction. In order to overcome the problem in computer memory for extremely high resolution climate models, an alternate approach of nesting LAM in GCM (e.g., Giorgi and Mearns 1991; Kida et al. 1991) has been developed in the study of limited area climate models. The nesting procedure can be implemented in a one-way or a two-way interactive mode. In the former, information from the coarser resolution model is used to drive the higher-resolution submodel, but information from the higher-resolution subregion does not feed back into the lower-resolution domain. In the latter, the exchange of information between the lower-resolution and higher-resolution model components occurs interactively and in both directions. The nested LAM-GCM models are mostly based on the one-way nesting procedure: most of the nested LAM-GCM models assume that the up-scale energy transfer from the higher-resolution submodel to the lower-resolution model can be ignored. This cannot be justified unless the magnitude of the scale interactions (i.e., zonal-wave and wave-wave interactions) is quantified to be small enough.

The purpose of the present study is to identify characteristic biases of the energy transformations in climate models simulated with different horizontal resolutions. We examine the effect of the artificial spectral truncation of the model atmosphere upon the energy redistribution in the wave number domain. The analysis of energy transfer spectra provides some useful information for studies of nesting LAM to GCM. For that purpose, it is desirable that the models are integrated under the same conditions. A sequence of climate model integrations is performed at NCAR using CCM2 under the same conditions, except for the parameters in the cloud parameterization (see Hack et al. 1993; Williamson 1993). Such a sequence of long term integrations was supported by the Model Evaluation Consortium for Climate Assessment (MECCA) project (MECCA Experiment and Analysis Plan 1991). The CCM2 simulations employed in the present study have horizontal resolutions of rhomboidal-15 (R15), and triangular-42, -63, and -106 (T42, T63, and T106). For comparison, the same energetics analysis is carried out for the observed atmosphere provided by the European Centre for Medium Weather Forecasts (ECMWF). The characteristic biases are presented for these climate models in comparison with the ECMWF global analysis.

2 Data

2.1 Model atmospheres

The NCAR CCM2 was extensively redesigned and recoded from earlier versions of the CCM in order to produce a state-of-the-art atmospheric GCM which is easy to use and to modify. The algorithms defining the CCM2 are detailed in Hack et al. (1993). This technical note also provides a complete list of references to papers that provide the developmental background for many of the components in the CCM2. Aspects of the CCM2, dynamic, thermodynamic, and radiative climate statistics are documented in Hack et al. (1994) and Kiehl et al. (1994).

In this study, four versions of the CCM2 with different horizontal spectral resolutions are analyzed: the CCM2-R15, -T42, -T63, and -T106. The longitude-latitude grid intervals of the R15, T42, T63, and T106 are approximately $7.5° \times 4.5°$, $2.8° \times 2.8°$, $1.9° \times 1.9°$, and $1.1° \times 1.1°$, respectively. These CCM2 datasets are analyzed after an interpolation from hybrid 18-layer into pressure 12-layer vertical coordinates (1000, 850, 700, 500, 400, 300, 250, 200, 150, 100, 70, 50 hPa). The energetics analysis is carried out during northern winter and summer in a tenth model year of a 10-year R15 run, in a tenth year of a 20-year T42 run, in a fifth year of a 5-year T63 run, and during January and July in a fourth model year of a 4-year T106 run, respectively. Only one year of data is analyzed for each resolution because the year-to-year variation is known to be sufficiently small for global energetics, according to our parallel study of the normal mode energetics analysis for 1985 to 1994 (see Tanaka and Kimura 1996). These history datasets were written once per model day and obtain data averaged over the preceding 24 hours.

2.2 Observed atmosphere

The characteristic biases of the climate models are investigated, comparing with the observed atmosphere. In this study, ECMWF global analysis (TOGA Basic Level III) from 1986 to 1990 is used as the observed atmosphere. The grid interval of the ECMWF analysis is $2.5° \times 2.5°$ and the corresponding maximum zonal wave number is 72. The datasets are the products of the uninitialized objective analyses with T106 model, but the vertical p-velocity is provided from the assimilation cycle. Thus, the vertical motion is not wholly consistent with the rest of the analysis field.

The assimilation system has been changing over the 5 years of the data used. However, none of the changes were fundamental for the TOGA dataset. Tanaka and Ji (1995) compared the original and reanalysis of the ECMWF, and Tanaka and Kimura (1996) compared the ECMWF TOGA dataset with other major global analysis by NMC and JMA in reference to the FGGE reanalysis.

Although the ECMWF assimilation models for the period of 1985–90 tend to underestimate the divergent flow and thus the vertical motion, the ECMWF TOGA analysis may be still considered as sufficient to compare with the simulated atmospheres. It is desired in future to use the reanalysis dataset to further discuss the discrepancies between the simulations and observations.

While the CCM2 datasets are archived in the form of daily means, the ECMWF analysis data consist of twice-daily values (0000Z, 1200Z). For this reason, it may be difficult to directly compare the energetics in detail for the CCM2 and the ECMWF analysis. Thus, we computed daily-mean values of the ECMWF analysis by averaging the twice-daily data. Although the results with daily-mean (this study) and twice-daily values (past studies) show minor differences, the use of the daily-mean datasets may be sufficient to compare the model atmospheres with the observed atmosphere.

3 Scheme of spectral energetics analysis

For the global energetics analysis, the computations in this study are based on standard methods of spectral energetics in terms of a one-dimensional wave number decomposition after Saltzman (1957, 1970). Here, all meteorological variables are expanded in zonal harmonics and substituted in the governing equations. Since the details of the analysis scheme are available in the preceding reports (Kung and Tanaka 1983), only an abbreviated description of the energy equations is presented here.

The one-dimensional wave number equations of kinetic energy and available potential energy by Saltzman may be written as

$$\frac{\partial K_M}{\partial t} = \sum_{n=1}^{N} M(n) + C(P_M, K_M) - D(K_M), \quad (1)$$

$$\frac{\partial K(n)}{\partial t} = -M(n) + L(n) + C(n) - D(n), \; n = 1,2,3, \ldots, \quad (2)$$

$$\frac{\partial P_M}{\partial t} = -\sum_{n=1}^{N} R(n) - C(P_M, K_M) + G(P_M), \quad (3)$$

$$\frac{\partial P(n)}{\partial t} = R(n) + S(n) - C(n) + G(n), \; n = 1,2,3, \ldots, \quad (4)$$

where the symbols K and P denote kinetic energy and available potential energy (refer to Table 1 for definitions of the variables). All quantities represent integrals over the total mass of the atmosphere. In this study, the limit of integration for the vertical totals is from the surface to 50 hPa. Noting that $\sum_{n=1}^{\infty} L(n) = 0$; $\sum_{n=1}^{\infty} S(n) = 0$, the equations of eddy kinetic energy and available potential energy may be obtained by summing Eqs. (2) and (4) from $n = 1$ to N, where N is the maximum zonal wave number for the analysis:

$$\frac{\partial K_E}{\partial t} = -M(K_E, K_M) + C(P_E, K_E) - D(K_E), \quad (5)$$

$$\frac{\partial P_E}{\partial t} = R(P_M, P_E) - C(P_E, K_E) + G(P_E). \quad (6)$$

Table 1. Symbols, definitions and variables

t	Time
n	Zonal wave number
N	Maximum zonal wave number
K	Kinetic energy
K_M	Zonal mean kinetic energy
K_E	Zonal eddy kinetic energy
$K(n)$	Kinetic energy at wave number n
P_M	Zonal mean available potential energy
P_E	Zonal eddy available potential energy
$P(n)$	Available potential energy at wave number n
$M(K_E, K_M)$	Conversion from K_E to K_M
$M(n)$	Conversion from $K(n)$ to K_M
$C(P_M, K_M)$	Conversion from P_M to K_M
$C(P_E, K_E)$	Conversion from P_E to K_E
$C(n)$	Conversion from $P(n)$ to $K(n)$
$L(n)$	Converison of K_E from all wave numbers to $K(n)$
$R(P_M, P_E)$	Conversion from P_M to P_E
$R(n)$	Conversion from P_M to $P(n)$
$S(n)$	Conversion of P_E from all wave numbers to $P(n)$
$D(K_M)$	Dissipation of K_M
$D(K_E)$	Dissipation of K_E
$D(n)$	Dissipation of $K(n)$
$G(P_M)$	Generation of P_M
$G(P_E)$	Generation of P_E
$G(n)$	Generation of $P(n)$

A set of equations is reduced to that derived by Lorenz (1955) and reviewed by Oort (1964) under the name 'space domain equations'. In Eqs. (1)–(6), dissipation of kinetic energy and generation of available potential energy are obtained as residual terms to balance the respective equations.

By evaluating these energetics terms, Saltzman showed, first, that the atmospheric kinetic energy is generated at the synoptic scale of zonal wave number 6–10 by baroclinic instability, and that the energy is transferred to both planetary waves and short waves. The energy transfer toward the short waves corresponds to the down-scale energy cascade to the dissipation range, whereas the transfer toward the large-scale (up-scale cascade) feeds the energy of the planetary waves and zonal jet stream in the atmosphere.

4 Results of the analysis

4.1 Meridional distributions of energetics terms

First, meridional distributions of kinetic energy and its transformations are compared for the CCM2 and ECMWF datasets during the northern winter and summer. Hereafter, the northern winter and summer represent the periods from December through February and June through August, respectively, except for CCM2-T106 which uses the monthly means for January and July.

Figure 1 illustrates the meridional distributions of zonal mean kinetic energy K_M, eddy kinetic energy K_E, zonal-wave interactions of kinetic energy $M(K_E, K_M)$, the eddy baroclinic conversion $C(P_E, K_E)$ for the CCM2 and ECMWF during the northern winter and summer. The error bars for the ECMWF represent a standard deviation

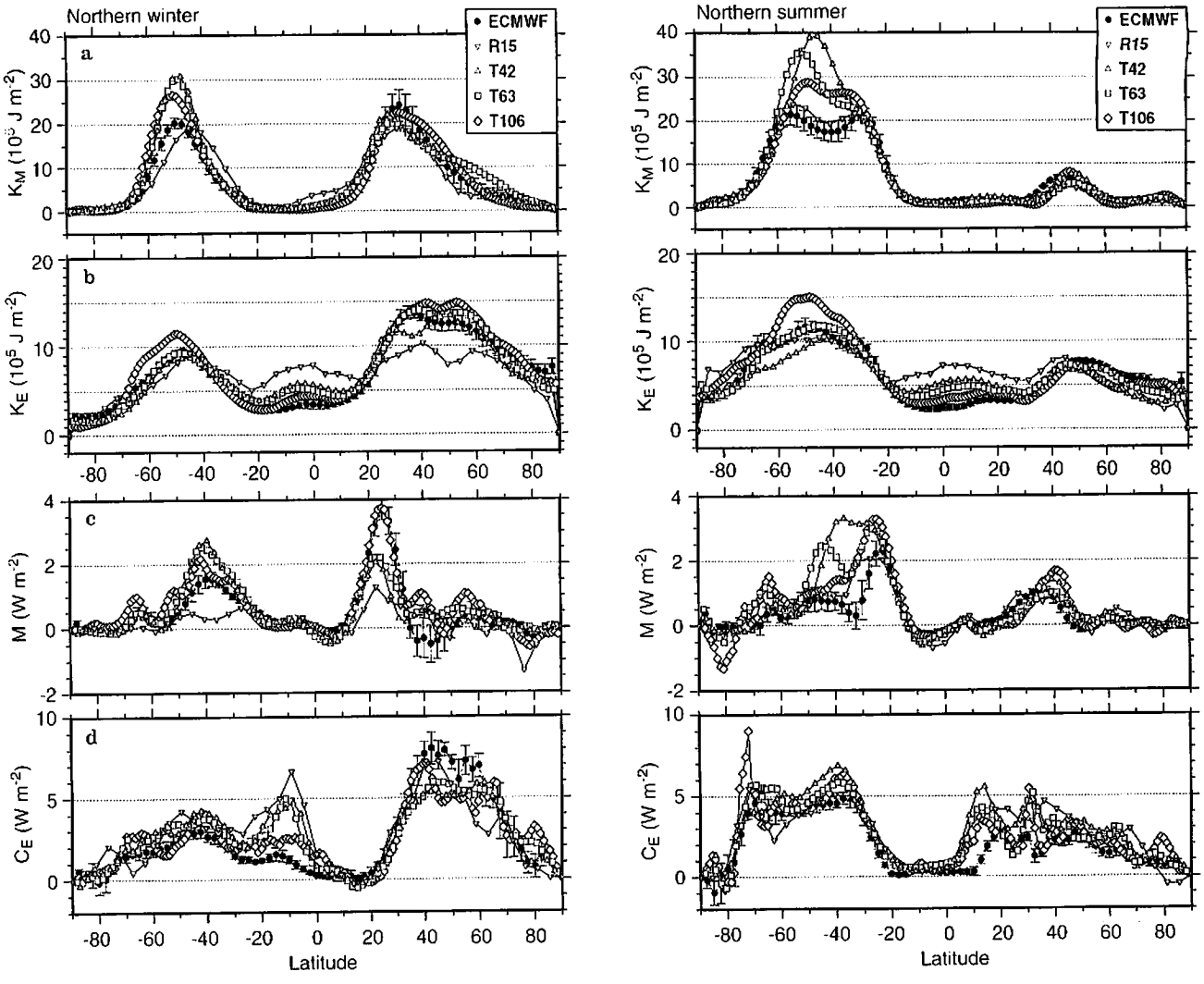

Fig. 1a–d. Latitudinal distribution of **a** K_M, **b** K_E, **c** $M(K_E, K_M)$ and **d** $C(P_E, K_E)$ for CCM2 and ECMWF datasets during the northern winter and summer

during the 5-year analysis period. The regional differences between the ECMWF analysis and CCM2 simulations are evident for these energetics terms.

Excessive zonal mean kinetic energy K_M in the CCM2 is analyzed in the Southern Hemisphere (SH), implying too strong a jet in the model. The larger K_M in the simulations is more evident in the winter SH compared with that in the summer SH. During the southern winter the ECMWF analysis indicates the double jet structure associated with the subtropical jet and polar frontal jet. These features are totally missing in T42, although the situation is improving in T106.

The eddy kinetic energy K_E for CCM2 is consistently larger than that of the ECMWF in the tropics. The discrepancy is improved with increasing model resolution. In addition, K_E for R15 is too small in winter hemisphere. The latitudinal distribution of K_E for R15 is flat compared with other CCM2 resolutions and ECMWF. Although K_M is improving as mentioned, K_E for T106 is too large in the SH for both seasons, which shows the difficulty of reproducing the SH circulation even in the higher resolution model.

Zonal-wave interactions of kinetic energy $M(K_E, K_M)$ in the CCM2 are larger than ECMWF in the SH; i.e., the CCM2 transfers too much energy from eddies to the zonal mean field to intensify the westerlies. The values of $M(K_E, K_M)$ at 40 °S in the southern winter are larger in CCM2 than ECMWF, which leads to the mismatch in the double-jet structure.

The eddy baroclinic conversion $C(P_E, K_E)$ for CCM2 is underestimated in the winter Northern Hemisphere (NH), whereas it is overestimated in the winter SH. A marked discrepancy of excessive $C(P_E, K_E)$ in CCM2 is noticed at 10 °S in the southern summer and at 10 °N in the northern summer, where the Intertropical Convergence Zone (ITCZ) locates. Hack et al. (1994) pointed out that the CCM2 has a noticeable bias in producing too much rainfall, the vast majority of which falls in the form of convective precipitation, especially in the topics. It is likely that the excessive $C(P_E, K_E)$ in the tropics causes too much precipitation along the ITCZ in CCM2.

Although the high resolution models indicate a better fit, in general, with observations, and the R15 is clearly inferior to the others, there is no evidence that the higher

resolution model is always better than the lower resolution model as far as the energy distributions are concerned.

4.2 *Spectral distributions of kinetic energy*

Spectral distributions of kinetic energies are illustrated in Fig. 2 for the CCM2 simulations and the ECMWF analysis in the wave number domain for the northern winter and summer. Figure 2a shows that the spectrum is approximately white for wave numbers 1 to 5, and it shifts to -3 power slope beyond the wave number 5. The -3 power slope is regarded as the characteristic of a 2-dimensional turbulence of enstrophy cascading to the inertial subrange (Kraichnan 1967; Leith 1968). The CCM2 spectrum coincides with that of ECMWF except for R15 which indicates higher biases in the energy level near the truncation wave number.

Figure 2b illustrates a spectrum of the coefficient of variation, defined as the standard deviation of temporal variations during the analysis period divided by their time average. The largest value of the coefficient of variation is about 40% at the synoptic scale, implying a large temporal variation of the energetics term around its mean value at this scale. The values are reduced to about 30% for the planetary waves and to 10% for short waves. The coefficient of variation for R15 is clearly biased from the observations, indicating less variation over almost all wave numbers. This may be a typical example that the characteristics in time variation can be biased from reality, even though the climatology can be well tuned at the right order for low-resolution models.

4.3 *Baroclinic conversion*

Figure 3 illustrates the spectral distributions of baroclinic conversion $C(n)$ for CCM2 and ECMWF datasets during the northern winter and summer. According to the result for ECMWF, the baroclinic conversion shows one peak at planetary waves and another peak in synoptic waves. The $C(n)$ for R15 is twice that of ECMWF at wave number 5 for northern summer. The $C(n)$ for CCM2 tend to improve as the model resolution increases.

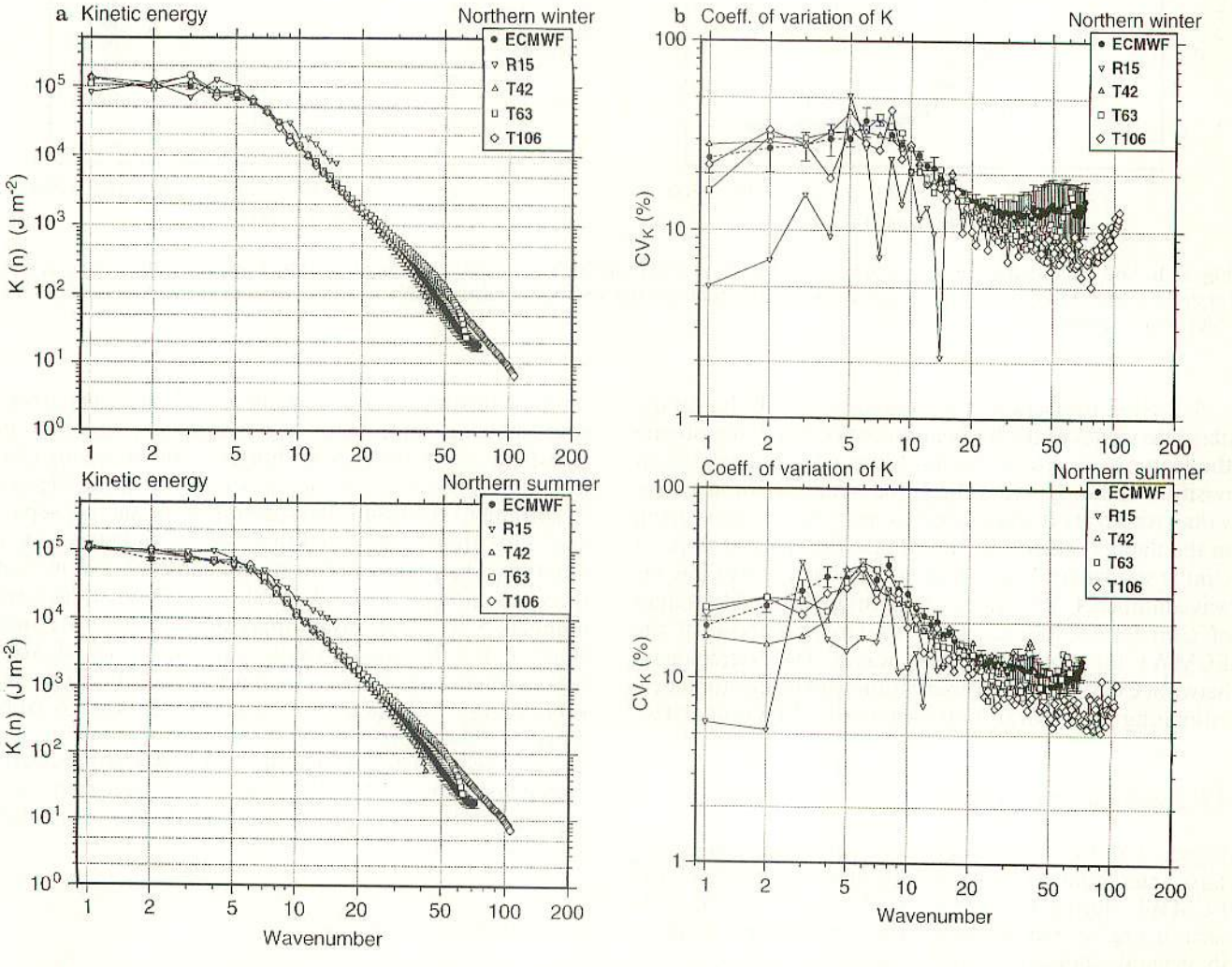

Fig. 2a, b. Spectral distribution of **a** kinetic energy and **b** coefficient of variation of $K(n)$ for CCM2 and ECMWF datasets during the northern winter and summer

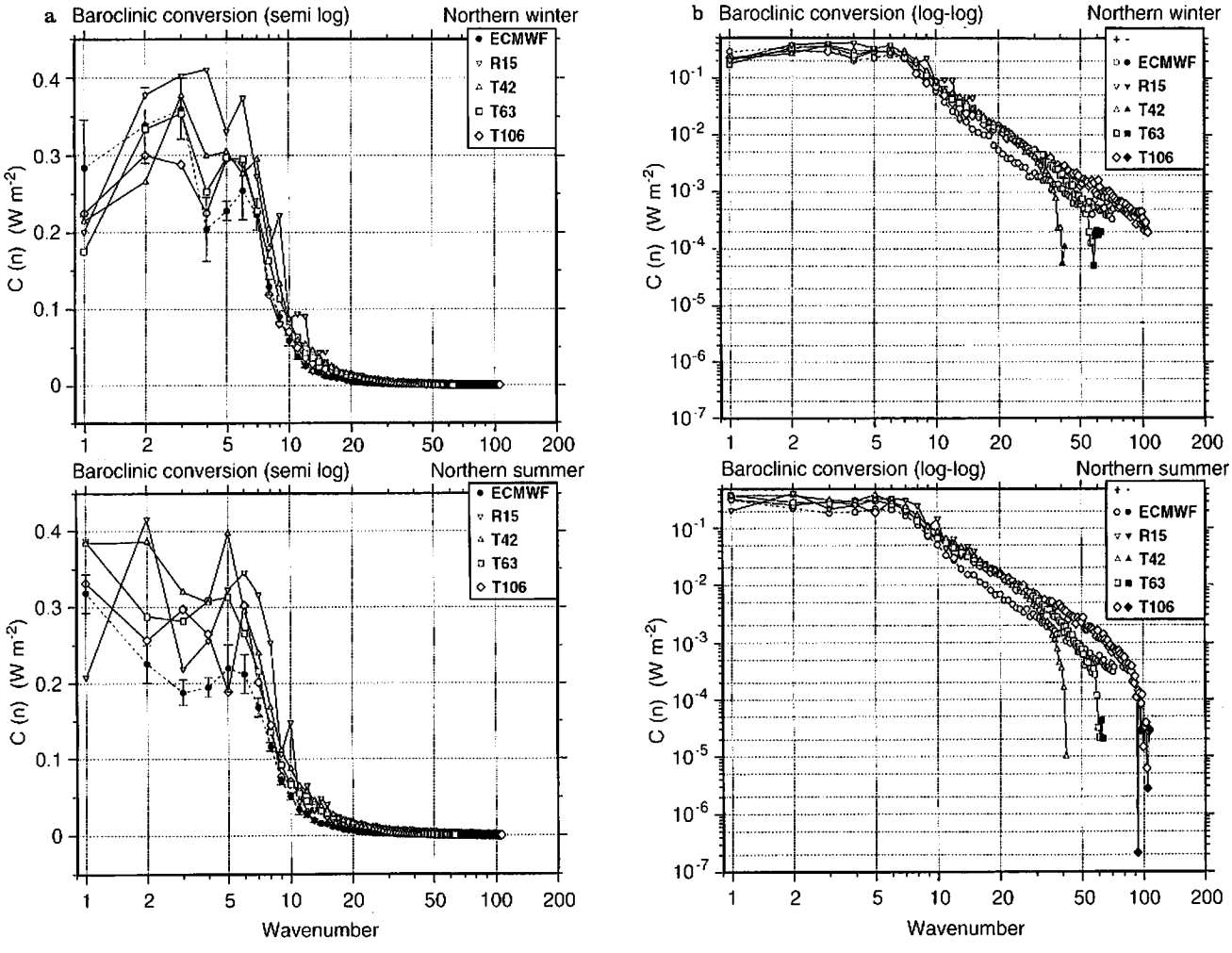

Fig. 3a, b. Spectral distribution of baroclinic conversion for CCM2 and ECMWF datasets during the northern winter and summer: **a** semi log and **b** log-log projection. A log–log projection takes absolute value of $C(n)$ and distinguishes negative values (*solid symbols*) from positive values (*open symbols*)

A log-log projection is presented in Fig. 3b by taking absolute values of the baroclinic conversion to investigate the features at shorter waves. Since $C(n)$ can take both positive and negative values, the symbols for negative values (solid) are distinguished from positive values (open) in the figures. The result shows that the spectral slope of $C(n)$ is similar to that of $K(n)$ indicating a power law for wavenumbers from synoptic to shorter waves. The values of $C(n)$ for CCM2 are twice as large as those of the ECMWF for synoptic to short waves. The discrepancies between CCM2 and the observations can be due to underestimating the vertical motion in the ECMWF analysis.

4.4 Zonal-wave interactions

Figure 4 illustrates the spectral distributions of zonal-wave interactions $M(n)$ of kinetic energy for CCM2 and ECMWF during the northern winter and summer. As seen in Fig. 4a, kinetic energy transformation is positive, in general, indicating the energy transformation from eddies to zonal-mean component. Namely, zonal mean kinetic energy is maintained by the energy supply from synoptic disturbances. The result for R15 is rather erroneous showing some large negative values. In order to investigate the properties at shorter waves, a log-log projection is presented in Fig. 4b for $M(n)$ as in Fig. 3b. According to the result, the spectral properties are separated into three ranges: $n = 1$ to 5, 5 to 25, and higher wave numbers. The values of $M(n)$ are about 5×10^{-2} W m^{-2} at the wave numbers 1 to 5. The values decrease at the wave numbers 5 to 25, showing approximately a -4 power slope. It is interesting to note that the values of $M(n)$ beyond the wave number 25 are negative, indicating a reverse energy transformations from zonal-mean to eddy motions. Such opposite energy transformations are not documented in the previous studies. Except for the clearly biased spectrum of R15, the results for higher resolution models coincide with observation for the wave numbers 5 to 25.

4.5 Wave-wave interactions

Figure 5a illustrates the spectral distributions of wave-wave interactions $L(n)$ for CCM2 and ECMWF during

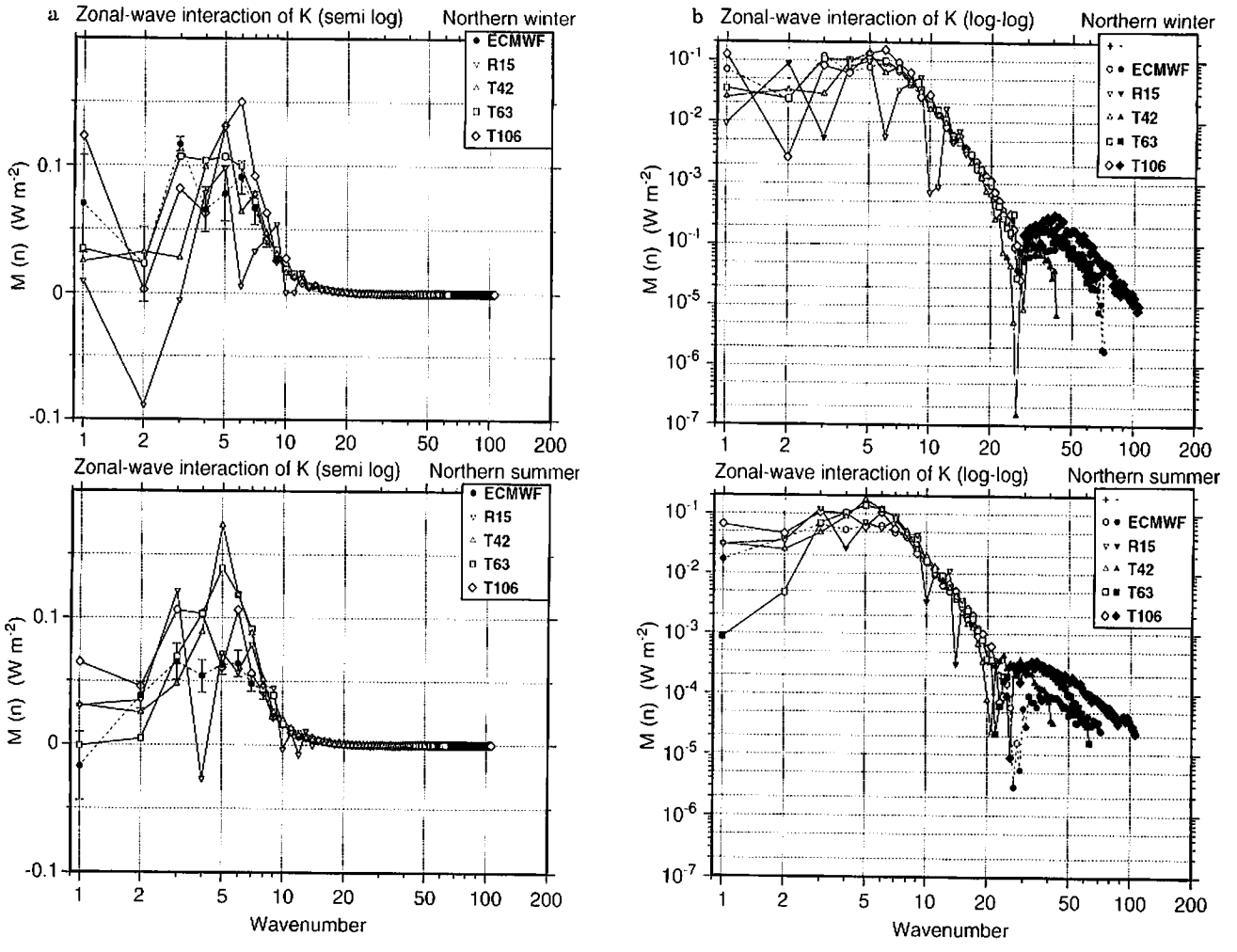

Fig. 4a, b. Spectral distribution of zonal-wave interactions of K for CCM2 and ECMWF datasets during the northern winter and summer: **a** semi log and **b** log-log projection

the northern winter and summer. This term is important to assess the magnitude of the scale interactions between the global- and regional-scale motions. The term is negative (solid symbols in Fig. 5a) at the synoptic waves, indicating that the energy is drawn from this range to other spectral domains. The baroclinic conversion is the main energy supply for the synoptic waves which compensates the loss of the negative $L(n)$. The values of $L(n)$ are positive both in planetary waves and short waves, indicating that the energy is transferred from the source range to both planetary waves and short waves. The energy transfer from synoptic waves to planetary waves is referred to as up-scale energy cascade, whereas the transfer to short waves is the down-scale energy cascade. In theory, the wave-wave interactions must vanish when summed over all waves from one to infinity, as expected from the energy conservation properties of a dynamic model. This restriction holds even for the truncated model atmosphere. Hence, the important down-scale energy cascade is forbidden when the wave number is truncated in the model atmosphere, for example, at the wave 15 for R15. As a result, the wave-wave interactions for R15 model show that the negative values in small wave numbers are compensated by the unrealistic positive values at wave numbers 10–15. The wave–wave interactions for R15 are markedly biased from those in ECMWF and other CCM2 for all wave number ranges, since the energy redistribution must be completed within the resolvable wave numbers. Accordingly, the energy redistribution is seriously distorted by the artificial spectral boundary at R15. For short waves, the down-sale energy cascade is overestimated for T42, T63, and T106 compared with the observation, although the values are converging to the observation as the resolution increases.

The distortion of the wave–wave interactions becomes clearer when the interaction terms are integrated with respect to the wave number. The integral function is regarded as an energy flux in the wave number domain. Since the summation of the interactions for all waves becomes zero as mentioned before, the energy flux will converge to zero as the wave number approaches infinity. This physical constraint is attained at the finite wave numbers when a model atmosphere is truncated at a finite wave number. Figure 5b illustrates the energy flux over the wave number domain evaluated for CCM2 and ECMWF during the northern winter and summer. The

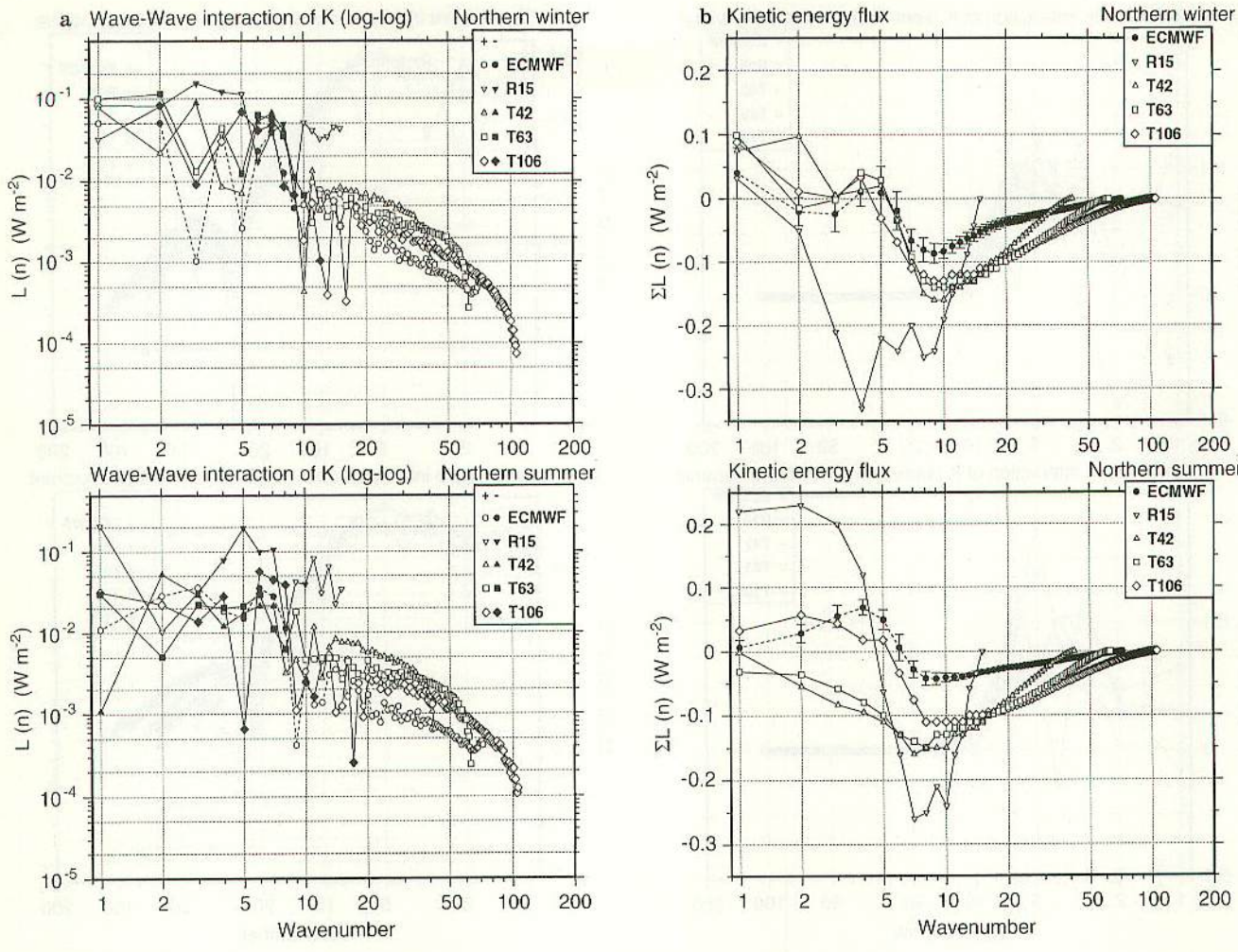

Fig. 5a, b. Spectral distribution of **a** wave-wave interactions of K and **b** kinetic energy flux $\sum L(n)$ for CCM2 and ECMWF datasets during the northern winter and summer

positive and negative values imply that the energy is transferred toward smaller and larger wave numbers (larger and smaller scales), respectively. The flux divergence should balance with an energy source there, whereas the flux convergence should balance with an energy sink. Evidently, there is a large energy source due to the baroclinic instability at the synoptic scale (see the northern summer case) near the zero crossing of the line where the flux strongly diverges. The results for the CCM2 qualitatively indicate distributions of the flux similar to those of ECMWF, but the magnitudes are twice larger for T42, T63, and T106. The distortion of the energy flux in R15 atmosphere is serious. The higher resolution models indicate a peak of the down-scale energy flux at the wave number about 10. At wave number 15 these higher resolution models show the flux of about 0.1 $\mathrm{W\,m^{-2}}$. However, this flux is forced to zero in R15 beyond wave number 15. The discrepancy is adjusted by parameterization of strong diffusion. The up-scale energy cascade observed for the northern summer is missing in T42 and T63. Only T106 reproduces the up-scale energy cascade in the northern summer. Since low-frequency variabilities of planetary waves, such as blocking, are largely controlled by the up-scale cascade from synoptic disturbances, the missing energy supply for planetary waves in T42 and T63 can be an important deficiency needing further improvement.

4.6 Energy transformations in CCM2-T106 and ECMWF analysis

Figure 6 compares the spectral distributions of $C(n)$, $M(n)$, and $L(n)$ for CCM2-T106 and ECMWF for the northern winter and summer using the same log-log projection. As noted earlier, the negative values are marked by solid symbols since those energy transformations can take both positive and negative sign. The baroclinic conversion $C(n)$ is about an order of magnitude larger than $M(n)$ and $L(n)$ at wave numbers 1 to 6. The spectral slope seems to obey a -3 power law beyond the synoptic wave numbers. The zonal-wave interactions $M(n)$ are larger than the wave-wave interactions $L(n)$ in the synoptic scale. Conversely, $L(n)$ are larger than $M(n)$ for short waves. The intersect of $M(n)$ and $L(n)$ is seen at wave number about 15 with the value of approximately 5×10^{-3} $\mathrm{Wm^{-2}}$. The zonal-wave interactions of kinetic energy $M(n)$ change sign beyond

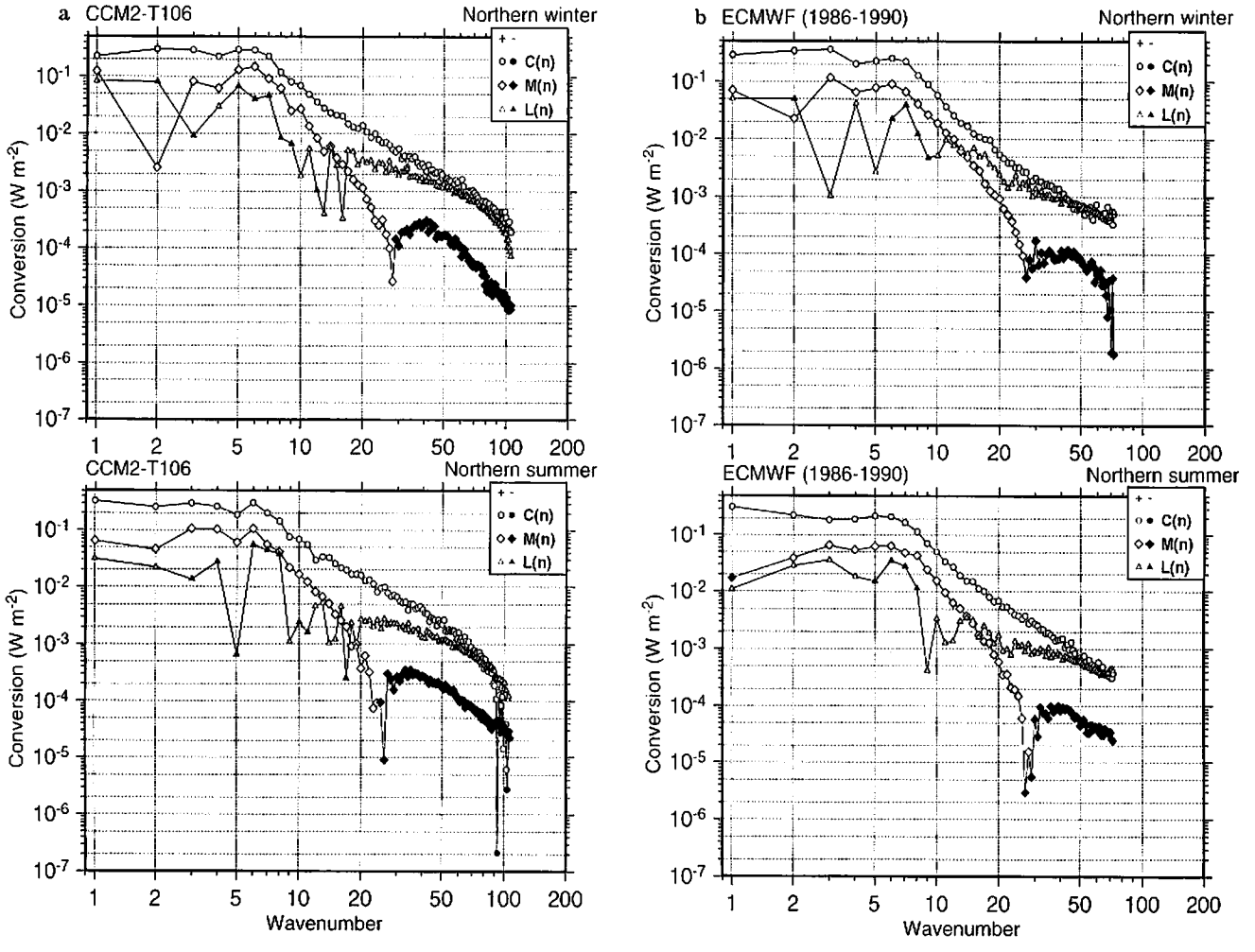

Fig. 6a, b. Spectral distribution of $C(n)$, $M(n)$, and $L(n)$ for **a** CCM2-T106 and **b** ECMWF datasets during the northern winter and summer. A log-log projection takes absolute values of $C(n)$, $M(n)$, $L(n)$ and distinguishes negative values (*solid symbols*) from positive values (*open symbols*)

the wave number 30, indicating an opposite energy flow from zonal-mean to eddy motions as mentioned before. The importance of this fact is considered in the Summary with respect to the search of the adequate model resolution.

4.7 Gross energy budget

Averaged zonal mean and eddy components of the energetics variables for the CCM2 and ECMWF are summarize in Table 2 for the northern winter and summer. The numbers in the round brackets in the column for the ECMWF analysis indicate the standard deviation (interannual variation) for 1986–1990.

Zonal mean and eddy components of kinetic energy K_M and available potential energy P_M in the CCM2 simulations are greater than those in the ECMWF by approximately 10%. The K_M and P_M in the CCM2 decrease and approach to those in the ECMWF as the model resolution increases. The improvement is mainly due to the reduction in the strength of the jet stream in the SH.

The $C(P_M, K_M)$ for CCM2 is nearly zero, compared with 0.5 W m^{-2} in ECMWF. This value was 1.3 W m^{-2} for the FGGE GFDL analysis (see Kung 1988). The $C(P_E, K_E)$ for CCM2 tends to decrease with increasing the resolution. This value was 3.1 W m^{-2} for the FGGL GFDL analysis. The same diagnostic analysis using the reanalysis data may provide a more realistic value of $C(n)$.

The $M(K_E, K_M)$ increases in the northern winter and decreases in the northern summer as the model resolution increases. The value of $M(K_E, K_M)$ is overestimated for CCM2 compared with the ECMWF. This value was only 0.25 W m^{-2} for the FGGE GFDL analysis. The $R(P_M, P_E)$, the zonal-wave interactions of available potential energy, are about 2.0 W m^{-2} for ECMWF, which are consistent with the FGGE GFDL analysis.

The intensity of the general circulation has been traditionally measured by the total generation of P, or the total baroclinic conversion from P to K, or the total dissipation of K. For the long-term average, the intensity of the general circulation has the following relations,

$$G(P_M) + G(P_E) = C(P_M, K_M) + C(P_E, K_E)$$
$$= D(K_M) + D(K_E).$$

Table 2. Global energy analysis with CCM2-R15, -T42, -T63, and -T106 and daily-mean ECMWF analysis for 1986–1990. Energy is in unit of 10^5 J m^{-2} and transformation in W m^{-2}

		NCAR CCM2				ECMWF
		R15	T42	T63	T106	1986–1990
K_M	Winter	8.06	8.88	8.77	8.35	7.65(0.32)
	Summer	7.12	8.88	8.17	7.78	7.07(0.12)
K_E	Winter	7.30	7.30	7.47	7.55	6.88(0.18)
	Summer	6.96	6.47	6.63	6.44	5.88(0.21)
P_M	Winter	46.71	57.39	55.33	52.81	51.47(0.88)
	Summer	43.97	56.93	53.12	47.09	47.46(1.02)
P_E	Winter	6.64	6.79	6.62	6.82	5.93(0.18)
	Summer	6.61	6.59	6.45	5.68	5.03(0.13)
$C(P_M, K_M)$	Winter	0.19	0.06	− 0.01	− 0.02	0.78(0.31)
	Summer	− 0.05	− 0.08	− 0.06	− 0.04	0.41(0.11)
$C(P_E, K_E)$	Winter	3.16	2.86	2.71	2.53	2.39(0.14)
	Summer	2.83	3.13	2.79	2.61	2.00(0.06)
$M(K_E, K_M)$	Winter	0.26	0.59	0.69	0.80	0.64(0.04)
	Summer	0.47	0.70	0.66	0.65	0.43(0.04)
$R(P_M, P_E)$	Winter	2.36	2.19	2.19	2.12	2.06(0.06)
	Summer	1.84	2.10	1.95	1.79	2.02(0.09)
$D(K_M)$	Winter	0.45	0.65	0.68	0.78	1.43(0.28)
	Summer	0.43	0.62	0.60	0.62	0.84(0.10)
$D(K_E)$	Winter	2.90	2.27	2.02	1.73	1.75(0.17)
	Summer	2.36	2.43	2.13	1.95	1.57(0.09)
$G(P_M)$	Winter	2.55	2.25	2.18	2.10	2.84(0.28)
	Summer	1.80	2.02	1.90	1.75	2.43(0.10)
$G(P_E)$	Winter	0.80	0.67	0.52	0.40	0.34(0.17)
	Summer	0.99	1.03	0.84	0.82	− 0.02(0.10)
$\sum_{n=0}^{N} C(n)$	Winter	3.35	2.92	2.70	2.51	3.17(0.43)
	Summer	2.78	3.05	2.73	2.57	2.41(0.12)

Since the terms $G(P_M)$, $G(P_E)$, $D(K_M)$, and $D(K_E)$ are obtained as the residual balance of the energy equations, the intensity of the general circulation is determined by $C(P_M, K_M) + C(P_E, K_E) = \sum_{n=0}^{N} C(n)$. The intensities measured with the ECMWF analysis are about 3.2 and 2.4 W m^{-2} for northern winter and summer, respectively. This value was 4.4 W m^{-2} for the FGGE GFDL analysis (see Kung and Tanaka 1983). The intensities of the CCM2 circulations seem to be reduced with increasing horizontal resolution.

5 Summary and discussion

The present study investigated the uncertainty associated with the horizontal resolutions in climate models. To evaluate the effect of a model's resolution on global energetics properties, comprehensive spectral energetics analysis is carried out for the NCAR CCM2 with different horizontal resolutions under the MECCA project. Both the energy spectrum and energy transformations in the wave number domain are investigated for the CCM2 over the truncation range of R15, T42, T63, and T106. For validation, we analyzed ECMWF global analysis for 5 year from 1986 to 1990. Special attention is given to the influence of the artificial truncation on the energy redistribution in the wave number domain of the model atmosphere.

Several discrepancies are found in the characteristics of the CCM2 and ECMWF. The CCM2 has difficulties in reproducing the circulation in the Southern Hemisphere, especially in southern winter. The westerly jet in the winter SH is too strong in the CCM2, and the simulation for the double-jet structure is not successful. These biases are due mostly to the excessive barotropic conversion $M(n)$ in this region.

The zonal mean component $C(P_M, K_M)$ of baroclinic conversion is too small and/or negative in the CCM2, while this term is positive in the ECMWF. In general, the energetics discrepancies between the CCM2 and ECMWF are significant in southern winter, reflecting the unrealistic features of the modeled winter Southern Hemisphere circulation.

Most of the discrepancies between the CCM2 and ECMWF resulted from enhanced synoptic disturbances in the CCM2 simulations. The simulated synoptic disturbances tend to transfer much more energy from $P(0)$ via $P(n)$ to $K(n)$, and further to $K(0)$. The eddy baroclinic conversion $C(n)$ for the CCM2 excessively enhances $K(n)$ in the middle latitudes of the SH. The barotropic conversion $M(n)$ for the CCM2 transfers too much kinetic energy from eddies to the zonal component especially in southern middle latitudes.

Previous studies showed that zonal mean kinetic energy is supplied by eddies in terms of the zonal-wave interactions of kinetic energy from eddies to zonal motions. According to our study, however, such an energy flow from eddy to zonal motions is valid only up to zonal wave numbers of about 30. We find that the zonal-wave interactions of kinetic energy change the sign beyond wave number 30 where the energy flow is from zonal to eddies for the high-resolution datasets of both ECMWF and CCM2-T106. This means that the large-scale zonal motions are diffusive against the short waves beyond wave

number 30, which may well be parameterized by various forms of the diffusion scheme. Conversely, we may infer from this result that the shorter waves with wave number lower than 30 are necessary to accurately represent the large-scale motions because these waves can actively influence the behavior of the zonal motions. Based on this finding, we suggest that the model resolution of T42 is the minimum requirement to adequately represent the general circulation.

According to the result from T106 simulation, the wave-wave interactions of kinetic energy show a down-scale energy transfer from synoptic waves to short waves. The energy flux in the wave number domain toward the short waves indicates a peak in magnitude at wave number about 10. Despite this fact, the down-scale energy transfer is forced to vanish at wave number 15 in R15 since the energy redistribution by the wave-wave interactions must be completed within the resolvable spectral range. Therefore, the energy flows in R15 are seriously distorted both in direction and size. The missing down-scale energy flux in R15 is parameterized by an increased diffusion process in order to draw the necessary amount of energy. Accordingly, the important and complicated two-way process of the scale interactions between global and local scales is treated as a prescribed one-way interaction in R15. Evidently, the model resolution of R15 is inadequate for climate studies from the energetics point of view.

In conjunction with the climate prediction by means of a limited area model (LAM) nested with the GCM such as R15, we can warn of a missing two-way interaction under the LAM-GCM. Both zonal-wave and wave-wave interactions of kinetic energy indicate the down-scale energy transfer beyond wave number 30. If the time average of these scale interactions are constant, or much larger than their time variations, the one-way interaction method may be valid for nesting LAM within GCM. However, if their time variations are comparable to time averages, a one-way nesting procedure is questionable. Even supposing that we attempt to save the computer resources of a T106 climate prediction by a nesting of LAM and R15, it would be difficult to obtain a similar prediction by these two approaches.

The improvements from R15 to T42 are significant in many respects, while the characteristics of T63 model are similar to those in T106 simulation. In practice, T42 seems to be sufficient as far as global energetics is concerned. This finding may be important for model construction, in the sense that T42 is the minimum requirement for the sufficient two-way interaction between eddies and zonal motions. This result is consistent with that described in Williamson et al. (1995). However, this conclusion should not be extended to regional features of climate models, especially those related to precipitation. As mentioned earlier, it is difficult in this study, to evaluate whether the magnitude of the small-scale vertical motions in ECMWF analysis is adequate or not. Since the baroclinic conversion is sensitive to the vertical motion, it is difficult to regard $C(n)$ for the ECMWF analysis as the representative one. It is desirable to carry out the same investigation using reanalysis data to provide a more reliable validation.

Acknowledgements. This research was supported by the MECCA project for the use of the NCAR CRAY and MSS. Partial support comes from the Central Research Institute of Electric Power Industry, Japan. Authors appreciate the help of Drs. J. Hack, D. Williamson, A. Kasahara and J. Tsutsui for their willingness to supply the CCM2 output and for valuable discussions. The technical assistance of Ms. K. Honda is appreciated.

References

Arpe K, Brankovic C, Oriol E, Speth P (1986) Variability in time and space of energetics from a long series of atmospheric data produced by ECMWF. Beitr Phys Atmos 59:321–355

Giorgi F, Mearns LO (1991) Approaches to the simulation of regional climate change: a review. Rev Geophys 29:191–216

Hack JJ, Boville BA, Briegleb BP, Kiehl JT, Rasch PJ, Williamson DL (1993) Description of the NCAR community climate model (CCM2). Technical Report NCAR/TN-382 + STR, Natl Cent Atmos Res

Hack JJ, Boville BA, Kiehl JT, Rasch PJ, Williamson DL 1994) Climate statistics from the National Center for Atmospheric Research community climate model CCM2. J Geophys Res 99:20785–20813

Kao SK, Chi CN (1978) Mechanism for the growth and decay of long- and synoptic-scale waves in the mid-troposphere. J Atmos Sci 35:1375–1387

Kida H, Koide T, Sasaki H, Chiba M (1991) A new approach for coupling a limited area model to a GCM for regional climate simulations. J Meteorol Soc Japan 69:723–728

Kiehl JT, Hack JJ, Briegleb BP (1994) The simulated earth radiation budget of the National Center for Atmospheric Research community climate model CCM2 and comparisons with the Earth Radiation Budget Experiment (ERBE). J Geophys Res 99:20815–20827

Kraichnan RH (1967) Inertial range in two-dimensional turbulence. Phys Fluids 10:1417–1423

Kung EC (1988) Spectral energetics of the general circulation and time spectra of transient waves during the FGGE year. J Clim 1:5–19

Kung EC, Baker WE (1986) Comparative energetics of the observed and simulated global circulation during the special observing periods of FGGE. Q JR Meteorol Soc 112:593–611

Kung EC, Tanaka H (1983) Energetics analysis of the global circulation during the special observation periods of FGGE. J Atmos Sci 40:2575–2592

Kung EC, Tanaka H (1984) Spectral characteristics and meridional variations of energy transformations during the first and second special observation periods of FGGE. J Atmos Sci 41:1836–1849

Leith CE (1968) Diffusion approximation for two-dimensional turbulence. Phys Fluids 11:671–672

Lorenz EN (1955) Available potential energy and the maintenance of the general circulation. Tellus 7:157–167

Manabe S, Stouffer RJ (1996) Low-frequency variability of surface air temperature in a 1000-year integration of a coupled atmosphere-ocean-land surface model. J Clim 9:376–393

MECCA Experiment and Analysis Plan (1991) Model Evaluation Consortium for Climate Assessment (MECCA). Techn Rep RP3267-2, Elect Power Res Inst

Oort AH (1964) On estimates of the atmospheric energy cycle. Mon Weather Rev 92:483–493

Saltzman B (1957) Equations governing the energetics of the larger scales of atmospheric turbulence in the domain of wave number. J Meteorol 14:513–523

Saltzman B (1970) Large-scale atmospheric energetics in the wave-number domain. Rev Geophys Space Phys 8:289–302

Tanaka HL, Ji Q (1995) Comparative energetics of FGGE reanalyses using the normal mode expansion. J Meteorol Soc Jap 73:1–12

Tanaka HL, Kimura K (1996) Normal mode energetics analysis and the intercomparison for the recent ECMWF, NMC, and JMA global analyses. J Meteorol Soc Jap 74:525–538

Tenenbaum J (1976) Spectral and spatial energetics of the GISS model atmosphere. Mon Weather Rev 104:15–30

Tsay CY, Kao SK (1978) Linear and nonlinear contributions to the growth and decay of the large-scale atmospheric waves and jet stream. Tellus 30:1–14

Williamson GS (1993) CCM2 datasets and circulation statistics. Techn Rep NCAR/TN-391+STR, Natl Cent Atmos Res

Williamson DL, Kiehl JT, Hack JJ (1995) Climate sensitivity of the NCAR Community Climate Model (CCM2) to horizontal resolution. Clim Dyn 11:377–397